A Variational Technique for Extracting Directional Spectra from Multi-Component Wave Data

ROBERT BRYAN LONG

Sea-Air Interaction Laboratory, Atlantic Oceanographic and Meteorological Laboratories, NOAA, Miami, FL 33149

KLAUS HASSELMANN

Max-Planck-Institut für Meteorologie, Hamburg, Germany

(Manuscript received 25 May 1978, in final form 4 August 1978)

ABSTRACT

The problem of extracting directional spectra from observed, multi-component wave data has two facets: 1) the observations provide information only on a finite number of integral properties of the wave field; hence the directional spectrum cannot be determined uniquely from the wave data alone; and 2) the observations contain statistical errors. These difficulties are dealt with by choosing an *optimal* directional spectrum model which simultaneously minimizes some integral property of the spectrum (its "nastiness") and passes an appropriate test of statistical significance. Although developed here in the context of surface wave directional spectra, the technique (adopted from the Backus-Gilbert inverse method) is applicable to any problem requiring the fitting of a model to data which represent integral properties of the function being modeled.

1. Model fitting techniques

Experiments designed to obtain direction-sensitive measurements of ocean wave spectra provide data which, in most cases, represent integral properties of the two-dimensional surface wave spectrum. These properties may be cast into the general form

$$\mathbf{d} = \int_0^{2\pi} d\theta S(\theta)\mathbf{b}(\theta), \tag{1}$$

where the components of the data vector $\mathbf{d}$ are weighted moments of the normalized directional distribution (spreading function) S defined by the kernel vector $\mathbf{b}$ (θ is the direction of wave propagation; the additional dependence of all quantities on wave frequency f has been suppressed). For example, an array of wave gages yields as basic data the set of cross spectra

$$E_{ij}(f) = \int_0^{2\pi} d\theta S(\theta,f)E(f) \times \exp[-ikr_{ij}\cos(\theta - \theta_{ij})] \tag{2}$$

between the ith and the jth wave record, where $E(f)$ is the one-dimensional surface wave spectrum, k is the wavenumber corresponding to f, and r_{ij} and θ_{ij} are the magnitude and direction, respectively, of the spatial displacement from the ith to the jth wave gage. Similarly, pitch/roll buoys provide time series of two orthogonal components of surface slope and vertical acceleration at a point on the sea surface; cross spectra between pairs of these records also have the form (1). Normalized versions of such cross spectra or linear combinations of them may be used to advantage in some situations, while still retaining the general form (1).

Given the data vector $\mathbf{d}$, extracting an estimate of the spectrum S requires the inversion of the set of integral equations (1). Normally, the inversion will not be unique, since the directional distribution is a continuous function, whereas the data set $\mathbf{d}$ is only of finite dimension.

One way to remove the indeterminacy is to restrict the model space to a finite dimensional subspace characterized by a parameter vector $\boldsymbol{\lambda}$ of dimension less than or equal to that of $\mathbf{d}$. A unique solution can then be obtained either by the method of least squares, if $\boldsymbol{\lambda}$ is of smaller dimension than $\mathbf{d}$, or by inverting (1) exactly, if the dimensions of $\boldsymbol{\lambda}$ and $\mathbf{d}$ are the same (and the model class is consistent with the data in the sense that a unique solution exists). The least-squares technique is usually favored as it yields stabler solutions. A basic disadvantage of the method is that the solutions fail to satisfy the data exactly, but this shortcoming generally appears less severe when the statistical errors of the data are taken into account. In fact, Eq. (1) represents a relationship between statistical quantities which can, in practice, never be known exactly.

0022-3670/79/020373-09$06.25

Physically realizable experiments can only provide estimates $\tilde{\mathbf{d}}$ of the true data $\mathbf{d}$, where

$$\tilde{\mathbf{d}} = \mathbf{d} + \boldsymbol{\epsilon}, \tag{3}$$

and $\boldsymbol{\epsilon}$ is a vector of random errors. Under the hypothesis that a given least-squares model S is the true spectrum [i.e., that it satisfies (1) exactly for the true data $\mathbf{d}$], the statistics of $\boldsymbol{\epsilon}$ can be computed. These may then be used to test whether the differences between the model prediction and the observed data $\tilde{\mathbf{d}}$ are statistically consistent with the expected errors. If this is the case, the optimal model is accepted as valid; if not, it is rejected. Olbers *et al.* (1976) have used this procedure successfully to extract statistically significant estimates of the three-dimensional internal wave spectrum in the main thermocline, using a model with approximately 20 free parameters, from 3660 cospectra and quadrature spectra obtained from a tetrahedral array of moored current and temperature meters.

A more fundamental shortcoming of the least-squares method, however, is that it provides no means, beyond statistical acceptance-rejection tests, to demonstrate that one model parameterization is superior to another—or even to define quantitatively what constitutes a superior model.

This consideration lies at the core of an alternative "inverse" technique, which appears to have been first suggested by Backus and Gilbert (1967). Instead of overcoming the underspecification of the model by (1) through the restriction of the model space to a dimension smaller or equal to that of the data vector, the number of integral restraints of the model is increased until the model again becomes overspecified. An optimal model can then be defined, as before, as the model which comes closest to fulfilling all requirements in some appropriate least squares sense. The additional integral restraints represent data-independent conditions which define, in effect, what is considered—subjectively, or on independent physical grounds—to be a "good" model. For example, in the case of directional spectra, the side condition $S(\theta) \geq 0$ must always be satisfied in addition to and independent of the data relation (1). The condition may be written in the integral form

$$\int_0^{2\pi} (S - |S|)^2 d\theta = 0. \tag{4}$$

Furthermore, one may seek a model which lies as closely as possible to a particular preferred model $\hat{S}(\theta)$, such as an isotropic distribution or, at the opposite extreme, a unidirectional spectrum. In this case one would require additionally

$$\int_0^{2\pi} (S - \hat{S})^2 d\theta = 0. \tag{5}$$

Alternately, one may seek the smoothest possible model by imposing the additional requirement

$$\int_0^{2\pi} \left[\frac{d^2S}{d\theta^2}(\theta)\right]^2 d\theta = 0. \tag{6}$$

Essential for the technique is that at least one of the additional conditions represents a positive definite form, such as (5) or (6), which normally cannot be satisfied simultaneously with the data. Thus, the model is overspecified, and one can define as the unique solution to the inverse problem the "optimal" model which minimizes some "error" expression formed from a suitable weighted combination of the various model equations, including both data conditions and additional constraints.

In most cases, more weight will be attached to the data conditions (1) than to subjective external conditions of the form (5) or (6). In fact, in the original Backus and Gilbert approach, Eqs. (1) were regarded as rigorous side conditions, and the "error" function was formed only from the external restraints. In view of the statistical indeterminacy of the data, however, some error in the data conditions can normally be accepted. Accordingly, we shall consider variable weightings for both data and external conditions and adjust the weighting such that the model satisfies the external conditions as closely as possible, while still remaining statistically consistent, within prescribed confidence limits, with the observed data. [However, the rigorous side condition (4) will always be satisfied exactly by assigning to this an essentially infinite weight.]

It may be remarked that no inverse technique can, of course, circumvent the basic difficulty of the underspecification of the continuous distribution by the finite data set. In all cases, a unique model can be constructed only by introducing more or less arbitrary additional restraints. The main advantage of the Backus-Gilbert inverse technique is that it defines clearly what is considered as a desirable or undesirable model property through the specification of an "error" function (more appropriately, "nastiness" function), the minimization of which defines the optimal model. This provides a tool for exploring the sensitivity of the model to alternative additional requirements, such as near-isotropy or near-unidirectionality, by considering alternative nastiness functions.

In the following sections, we shall examine the consequences of the application of the nastiness function based on the conditions (1), (4) and (5) to the problem of estimating directional spectra. An array of wave gages is considered as an example. Using artificially generated data, it is shown how the region of statistically acceptable solutions is affected by array geometry and the variability of the data estimates. Real data cases are also presented.

2. Defining the optimal model

Simultaneous consideration of the conditions (1), (4) and (5) suggests a nastiness function of the general form

$$\eta = \alpha \boldsymbol{\epsilon}^{\mathrm{T}} \mathbf{M} \boldsymbol{\epsilon} + \beta \int_0^{2\pi} d\theta (S - |S|)^2 + \int_0^{2\pi} d\theta (S - \hat{S})^2, \quad (7)$$

where

$$\boldsymbol{\epsilon} = \tilde{\mathbf{d}} - \int_0^{2\pi} d\theta S \mathbf{b} \quad (8)$$

is an n-dimensional column vector representing the errors between the observed data $\tilde{\mathbf{d}}$ and the model prediction, $\boldsymbol{\epsilon}^{\mathrm{T}}$ is its transpose, $\mathbf{M}$ is a positive definite symmetrical matrix, which will be defined below, and α and β are weighting factors. Since we wish to satisfy the condition (4) exactly, we shall consider (7) in the limit $\beta \to \infty$. [Formally, this turns out to be simpler than including (4) as an exact side condition and working with a Lagrange multiplier.]

The weighting factor α and the matrix $\mathbf{M}$ in the first term in the right-hand side of (7) determine the penalty one wishes to assign to a deviation between the observed data $\tilde{\mathbf{d}}$ and the model prediction, relative to the penalty for a deviation between the optimal model and the preferred model $\hat{S}$, as expressed by the last term. This will depend on the statistical errors associated with the observed data $\tilde{\mathbf{d}}$.

Consider the hypothesis that the optimal model obtained by minimizing η represents the true model, yielding the true data vector $\mathbf{d}$. One can then define an n-dimensional γ-probability region R around $\mathbf{d}$ such that $\int_R p(\tilde{\boldsymbol{\epsilon}}; \mathbf{d}) d\boldsymbol{\epsilon} = \gamma$, where $p(\boldsymbol{\epsilon}; \mathbf{d})$ is the probability of obtaining an error $\boldsymbol{\epsilon} = \tilde{\mathbf{d}} - \mathbf{d}$ in the estimation $\tilde{\mathbf{d}}$ of $\mathbf{d}$ for a particular data realization. If the data sample is not too small, the errors are approximately jointly Gaussian, i.e.,

$$p(\boldsymbol{\epsilon}; \mathbf{d}) = (2\pi)^{-n/2} |\mathbf{V}|^{-1/2} \exp\{-\tfrac{1}{2} \boldsymbol{\epsilon}^{\mathrm{T}} \mathbf{V}^{-1} \boldsymbol{\epsilon}\}, \quad (9)$$

where the error covariance matrix $\mathbf{V} = \langle \boldsymbol{\epsilon} \boldsymbol{\epsilon}^{\mathrm{T}} \rangle$ can be estimated using standard techniques of time series analysis (cf. Jenkins and Watts, 1968). The "true" data $\mathbf{d}$ predicted by the optimal model may then be regarded as statistically consistent with the observed data $\tilde{\mathbf{d}}$ at the γ-confidence level if $\tilde{\mathbf{d}}$ lies within R. To make the region R unique it is normally assumed that it is bounded by a surface of constant probability density or, equivalently, constant

$$\rho^2 = \boldsymbol{\epsilon}^{\mathrm{T}} \mathbf{V}^{-1} \boldsymbol{\epsilon}. \quad (10)$$

This definition yields the smallest region R for a given confidence level γ and is, in fact, the only definition which is invariant with respect to linear transformations of the data. The radius ρ_γ of R for given γ is readily determined by noting that the projection of the n-dimensional normal distribution (9) on to the variable ρ^2 yields a chi-square distribution with n degrees of freedom and standard normalization ($<\rho^2> = n$).

Complementary to R one can then define for a given data vector $\tilde{\mathbf{d}}$ the confidence region $\tilde{R}$ as the set of all true data $\mathbf{d}$ which are statistically consistent with $\tilde{\mathbf{d}}$. To the extent that $\mathbf{V}$ does not vary significantly over $\tilde{R}$, this is the same ellipsoid as R but with center at $\tilde{\mathbf{d}}$ instead of $\mathbf{d}$. Both regions R and $\tilde{R}$ are defined by the inequality

$$\rho^2 = \boldsymbol{\epsilon}^{\mathrm{T}} \mathbf{V}^{-1} \boldsymbol{\epsilon} = (\tilde{\mathbf{d}} - \mathbf{d})^{\mathrm{T}} V^{-1} (\tilde{\mathbf{d}} - \mathbf{d}) \leqslant \rho_\gamma^2, \quad (11)$$

with either $\mathbf{d}$ (in the case of R) or $\tilde{\mathbf{d}}$ (in the case of $\tilde{R}$) regarded as fixed.

Returning to the general structure of the nastiness function (7), we now consider the particular problem of determining the optimal model which has a minimal deviation from a favored model $\hat{S}$, satisfies the condition (4) exactly, and at the same time lies in the confidence region $\tilde{R}$ of $\tilde{\mathbf{d}}$, i.e., satisfies the inequality (11). Unless the favored model $\hat{S}$ itself is already consistent with the data, the minimal solution will normally lie on the surface of $\tilde{R}$, and we can therefore replace the inequality in (11) by an equality. The side condition (11) can then be incorporated in the nastiness function formed from the conditions (4) and (5) as an additional term multiplied by a Lagrange multiplier α. This yields the general form (7) with the matrix in the first term given by $\mathbf{M} = \mathbf{V}^{-1}$. We shall adopt this form for $\mathbf{M}$ in the following, thereby providing a simple statistical interpretation of the optimal model obtained by minimizing (7). The value of the Lagrange multiplier α for given ρ_γ is determined by the side condition (11). Numerically it is more convenient to reverse the procedure and use (11) to determine ρ_γ, given α. The appropriate value α for given ρ_γ can then be determined by iteration.

Taking the variation of Eq. (7) yields an equation for the minimal solution:

$$\delta\eta = \int_0^{2\pi} d\theta \{2(S - \hat{S}) + 4\beta(S - |S|) - 2\alpha \boldsymbol{\epsilon}^{\mathrm{T}} \mathbf{V}^{-1} \mathbf{b}\} \delta S = 0,$$

where we have used, from (8),

$$\delta\boldsymbol{\epsilon} = -\int_0^{2\pi} d\theta \mathbf{b} \delta S.$$

Since δS can be arbitrarily chosen, this requires

$$S(\theta) = \begin{cases} \hat{S} + \alpha \boldsymbol{\epsilon}^{\mathrm{T}} \mathbf{V}^{-1} \mathbf{b} & \text{for } S > 0 \\ (1 + 4\beta)^{-1} [\hat{S} + \alpha \boldsymbol{\epsilon}^{\mathrm{T}} \mathbf{V}^{-1} \mathbf{b}] & \text{for } S < 0. \end{cases}$$

In the limit as $\beta \to \infty$, the expression for negative

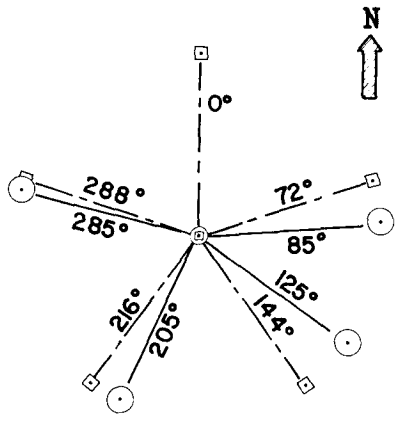

FIG. 1. Wave gage array geometries showing five-element North Sea array (⊙) and hypothetical six-element star array (⊡) used in some of the numerical experiments. The radius of both arrays is 90 m.

S approaches zero, and we obtain

$$S(\theta) = (\hat{S} + \mathbf{b}^T\boldsymbol{\lambda})H(\theta), \tag{12}$$

where

$$H(\theta) = \begin{cases} 1 & \text{if } (\hat{S} + \mathbf{b}^T\boldsymbol{\lambda}) > 0 \\ 0, & \text{otherwise} \end{cases} \tag{13}$$

and

$$\boldsymbol{\lambda} = \alpha\mathbf{V}^{-1}\boldsymbol{\epsilon}. \tag{14}$$

Substitution of (12) and (14) in the expression (8) for the error yields a set of equations for $\boldsymbol{\lambda}$:

$$\tilde{\mathbf{d}} = \alpha^{-1}\mathbf{V}\boldsymbol{\lambda} + \int_0^{2\pi} d\theta(\hat{S} + \mathbf{b}^T\boldsymbol{\lambda})H\mathbf{b}. \tag{15}$$

Once the coefficients $\boldsymbol{\lambda}$ are determined, S follows from (12) and (13). The solution of (15) represents a nonlinear problem because of the implicit dependence of H on $\boldsymbol{\lambda}$. Moreover, the covariance matrix $\mathbf{V}$ must be defined by the solution itself. However, a solution can be readily constructed numerically by the following iterative scheme: A zeroth-order guess at $\boldsymbol{\lambda}$ yields a zeroth-order solution for $S(\theta)$ and $H(\theta)$ through Eqs. (12) and (13). This function is used to estimate the covariance matrix $\mathbf{V}$ using standard spectral estimation formulas (cf. Jenkins and Watts, 1976). With $\mathbf{V}$ and H given, Eq. (15) represents a set of linear equations for $\boldsymbol{\lambda}$, the solution of which yields the first iteration for $\boldsymbol{\lambda}$, and so forth. An optimal solution is determined in this manner for fixed α. As indicated earlier, a second iteration loop is then needed to determine the α value corresponding to a given confidence limit ρ_γ. Experience with this scheme applied to wave gage arrays has shown convergence to be reasonably reliable and rapid. In some cases, the iteration in $\boldsymbol{\lambda}$ showed a tendency to overshoot, and better convergence could be achieved by replacing the new $\boldsymbol{\lambda}$ value at each iteration step by the mean of new and old values. The iteration in α was based on a linear interpolation/extrapolation scheme. Typically, seven $\boldsymbol{\lambda}$ iterations for fixed α and four or five α iterations were necessary to complete the solution to satisfactory accuracy.

3. Application to wave gage arrays

As a test, the inverse technique was applied to a five-element directional array of bottom pressure transducers deployed in the North Sea during JONSWAP 75. The measurements constituted a pilot project to measure the directional properties of swell in shallow water in order to distinguish between several possible mechanisms of swell decay (cf. Hasselmann *et al.*, 1973; Long, 1973; Shemdin *et al.*, 1979). Due to technical difficulties an originally planned array of instruments could not be completed in 1975 and the residual array (shown in Fig. 1) was not optimal. Nevertheless, the data provided a suitable case for testing the usefulness of the inverse technique under conditions of rather weak resolution often encountered in practice.

The data set consisted of all combinations of cross spectra and autospectra obtainable from the five instruments. The basic spectral estimates obtained by standard FFT methods from 20 min records had 18 degrees of freedom, a Nyquist frequency of 1 Hz, and a bandwidth of 1/128 Hz. To obtain higher statistical stability, however, three adjacent frequency bands were averaged, yielding 54 degrees of freedom at a resolution of 0.0234 Hz.

Writing the array equations (2) in the form

$$\frac{E_{ij}(f)}{E(f)} = \int_0^{2\pi} d\theta S(\theta,f) \times \exp[-ikr_{ij}\cos(\theta - \theta_{ij})], \quad i,j = 1,\ldots,m, \tag{16}$$

the basic data set $\mathbf{d}$ is seen to consist of the $m(m-1) = 20$ cospectral and quadrature spectral components of the normalized cross spectra E_{ij}/E, $i \neq j$; the m further equations for $i = j$ yield the single normalization condition

$$1 = \int_0^{2\pi} d\theta S(\theta,f). \tag{17}$$

This can also be treated formally as a data equation, the only difference from the other equations being that the statistical error of the data value 1 is identically zero. [A small formal complication arises because the matrix $\mathbf{V}$ becomes singular if this is done, whence the matrix $\mathbf{M} = \mathbf{V}^{-1}$ in (7) does not exist. For theoretical consistency in the development beginning with (7), Eq. (17) should be treated as an absolute constraint, rather than a data equation, and incorporated into η using another Lagrange multi-

plier. This and the vector λ, defined by (14), become the parameters of a model which is, in fact, identical to that obtained by formally treating (17) as a data equation and ignoring the resulting singularity of V. This complication is purely a formal question of interpretation without practical consequence since V need not be inverted in solving the final model equations (15).]

Computation of the elements of the covariance matrix V involves evaluation of the covariances of various estimates of cospectra and quadrature spectra, normalized in terms of the autospectra. Recipes for computing these covariances are given in Jenkins and Watts (1968, Appendix A9.1 and ¶ 3.2.5) in terms of the true cross spectra of the process; at the mth iteration, these are calculated by integrating (16) using $S = S^{(m)}$. An important property of V is that it is proportional to $1/\nu$, where ν is the degrees of freedom of the spectral estimators $\bar{E}_{ij}$.

The constraint $\rho^2 = \rho_\gamma^2$ is evaluated from a table of percentage points of the X_μ^2 distribution. Taking $\gamma = 0.8$ (the choice of γ is to some extent arbitrary; a smaller value has the same effect in the numerical cases studied as a larger number of degrees of freedom in the spectral estimates), we obtain for the five-element array of Fig. 1 [$\mu = m(m-1) = 20$, the side condition (17) not being counted], $\rho_\gamma^2 \approx 25$. For the hypothetical six-element array used in some of the numerical experiments below, $\mu = 30$ and $\rho_\gamma^2 \approx 36$.

4. Results for North Sea data

Some examples of optimal model fits for the North Sea array are shown in Fig. 2. Directional distributions were computed for a wind sea peak (Fig. 2a) [$f = 0.156$ Hz, wavelength = 60 m] and a swell peak (Fig. 2b) [$f = 0.109$ Hz, wavelength = 101 m], both taken from the same spectrum (Fig. 2c). For each data set, two favored models were tried, an isotropic form [$\hat{S} = 1/(2\pi)$] and one with a single lobe centered on the apparent dominant wave direction. The position and shape of the lobe were determined by a preliminary calculation which least-squares fitted a five-harmonic Fourier expansion of S in θ to the data set [the Fourier-Bessell technique of Barber (1963)]. The principal lobe of this fit was retained, the rest of the distribution set equal to zero, and the result renormalized and used as $\hat{S}$ in the subsequent analysis.

In both cases, the optimal model approaches the favored model $\hat{S}$ as closely as possible under the constraints set by the data. Thus a comparison of the optimal models for the two favored cases, which were chosen to represent fairly opposite extreme situations, should give some indication of which features of the directional distribution are fairly independent of and which are more strongly governed

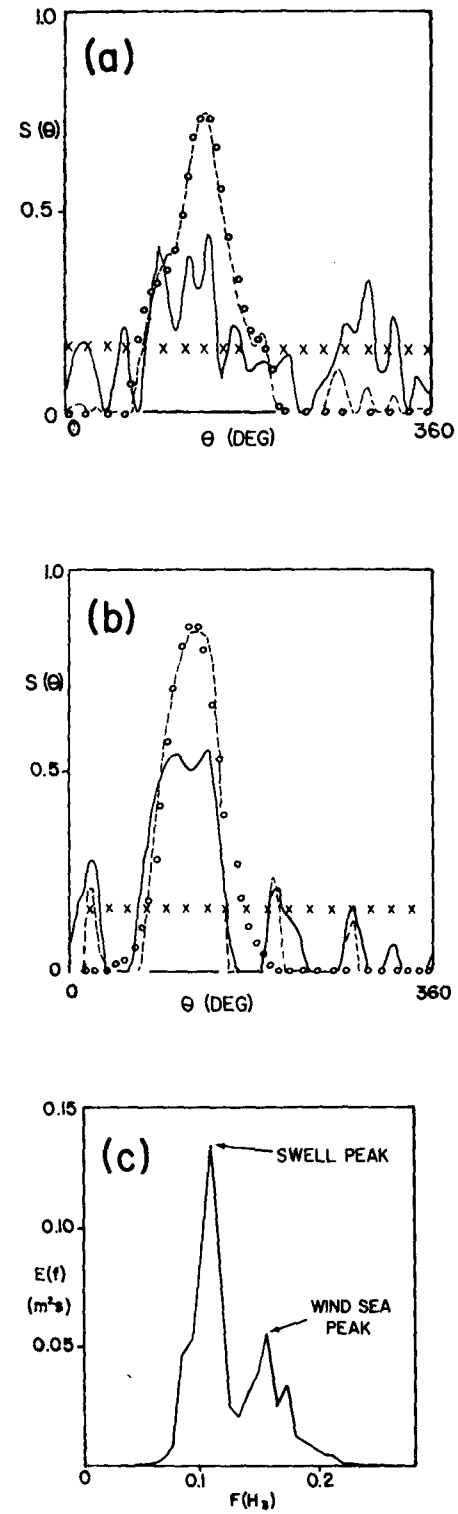

FIG. 2. Optimal spectral model fits to the North Sea data. Favored models (see text) are indicated by discrete points (×,○), the optimal fits by curves (solid and dashed, respectively): (a) example of a wind wave peak; (b) example of a swell peak (see text); (c) frequency spectrum indicating wind sea and swell peaks corresponding to cases (a), (b).

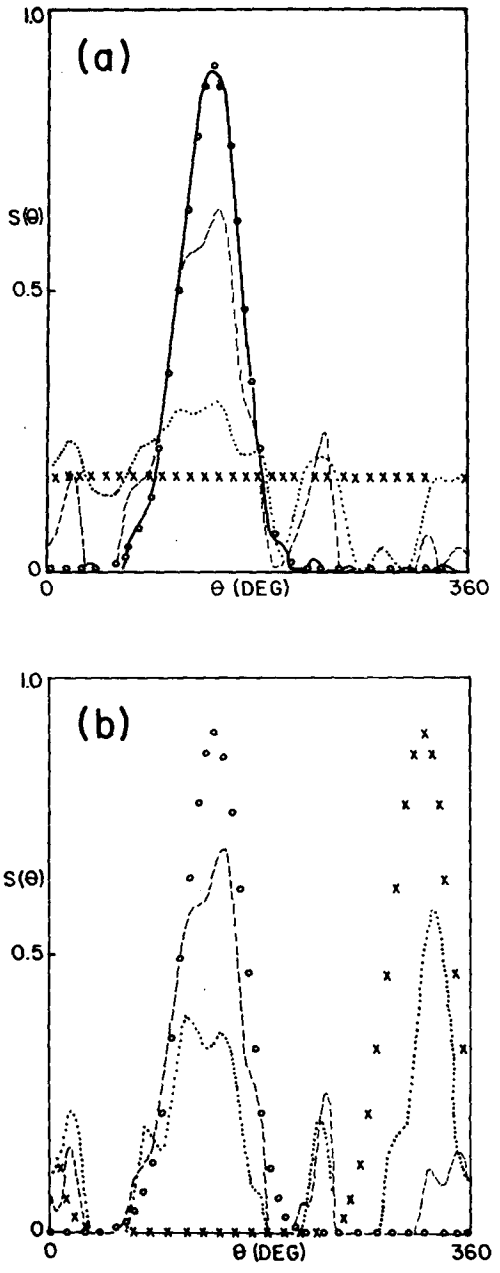

FIG. 3. Experiments with exact data. The input test spectrum S_W is indicated by the circles, the favored model $\hat{S}$ by the crosses. Optimal model fits are shown by curves: dotted lines, $\nu = 30$; dashed lines, $\nu = 180$; solid line, $\nu = \infty$. (a) Isotropic favored model, $\hat{S} = 1/2\pi$; (b) effect of misleading favored model, $\hat{S} = C_0 \cos^{20}[1/2(\theta - 317°)]$.

by the additional assumptions needed to invert the data set.

Despite the differences in $\hat{S}$, both optimal models reproduce the same principal features: 1) a principal lobe centered near the direction indicated by the Fourier-Bessell least-squares fit, and 2) spike-like side lobes. The former is believed to represent a directional maximum actually present in the wave field. The latter appear to result from a folding of this maximum by the antenna beam pattern of the array; the side lobes appeared in all spectra analyzed, independent of the choice of $\hat{S}$, and apparently represent a basic limitation of the array geometry. It should be noted in this context that the structure of the antenna beam pattern, defined by

$$G(k) = 1 + \sum_i \sum_{j \neq i} \exp(-i\mathbf{k} \cdot \mathbf{r}_{ij})$$

(Barber, 1963) is reflected in the optimal model itself, which has the form of an expansion—for positive S—in the same set of basis functions, $\exp(-i\mathbf{k} \cdot \mathbf{r}_{ij})$. Although the present technique generally yields higher directional resolution than the classical antenna beam method and avoids negative lobes, it appears that the problem of generating spurious (positive) side lobes is not entirely avoided.

5. Numerical experiments

To clarify this point, a set of numerical experiments was conducted to investigate the following specific questions:

(i) Given a set of exact, noise-free cross spectra from the five-element array of Fig. 1, what is the effect on the solution of varying degrees of freedom (i.e., varying confidence regions) and different choices for $\hat{S}$?

(ii) Given artificially generated data containing statistically consistent errors and no *a priori* knowledge (i.e., $\hat{S} = 1/2\pi$), how does the accuracy of the recovered solution respond to varying degrees of freedom in the spectral estimators and to changes in array geometry?

A test spectrum typical of a wind sea near the spectral peak (Mitsuyasu *et al.*, 1975)

$$S_W = C_0 \cos^{20}[1/2(\theta - 137°)]$$

(where θ is measured in degrees clockwise from north and C_0 is a normalization constant) was used for most of the numerical experiments. A second model,

$$S_S = C_1 + C_2 \cos^4(\theta - 54°) + C_3\{1 + \cos[18(\theta - 114°)]\} M(\theta),$$

consisting of a narrow 20° swell peak superposed on an undulating background, was also used. The swell component was represented by the last term containing the masking function

$$M(\theta) = \begin{cases} 1, & 104° \leq \theta \leq 124° \\ 0, & \text{otherwise.} \end{cases}$$

The constants C_1, C_2 and C_3 were adjusted so that one-third of the wave energy was in the swell peak and two-thirds in the background.

The wave frequency assumed in all cases corre-

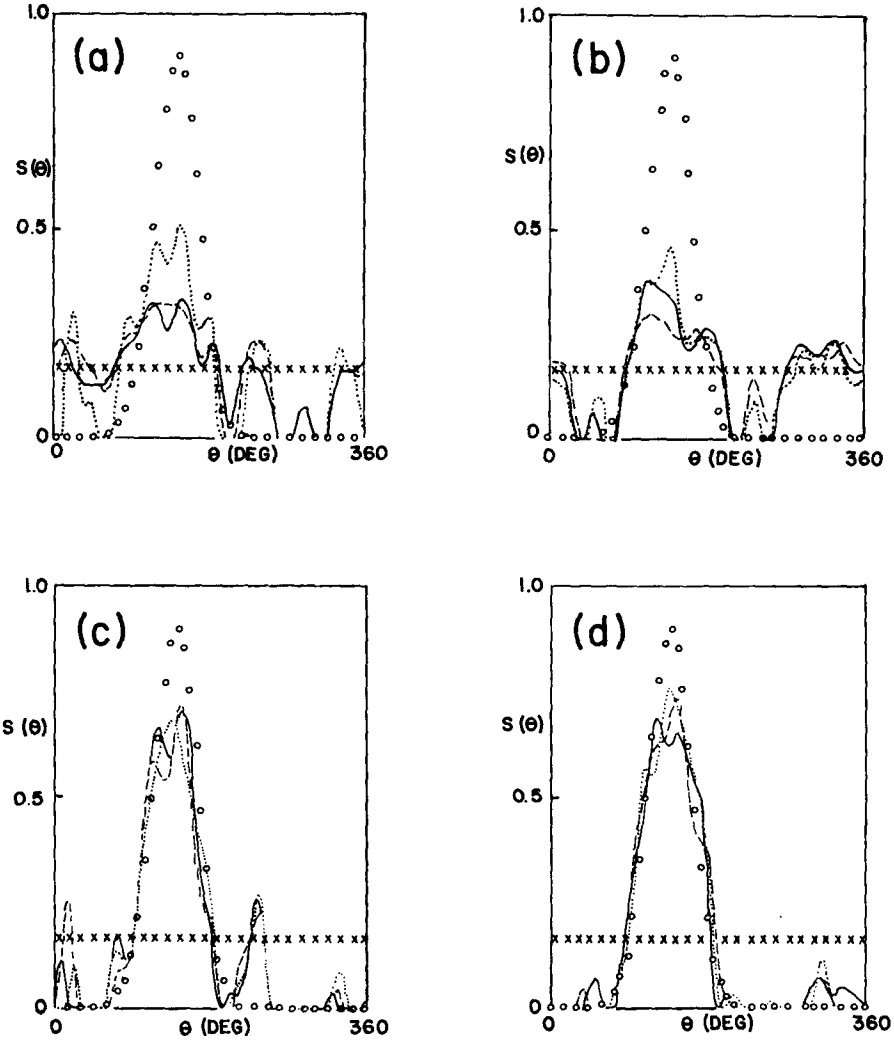

FIG. 4. Experiments with artificial noisy data. Input test spectrum S_W and favored model $\hat{S}$ are indicated by discrete points (○,×, respectively). Optimal model fits for three realizations are shown in each panel: (a) five-element array, $\nu = 30$; (b) six-element star array, $\nu = 30$; (c) five-element array, $\nu = 180$; (d) six-element star array, $\nu = 180$.

sponded to a wavelength of 100 m. For each experiment, the set of "true" cross spectra E_{ij} were calculated by numerically integrating (16) with $S = S_W$ or S_S. These results were used directly as "observed" data to investigate question (i). To investigate (ii), the "observed" data were formed by adding a set of statistically consistent errors to the "true" data. In generating the set of errors e allowance must be made for the fact that the components of e are not mutually independent (the covariance matrix V is not diagonal). This can be accounted for by representing e as a linear combination of the statistically orthogonal normalized eigenvectors of V. The coefficient of each eigenvector can then be generated independently by selecting a random number from a Gaussian population with zero mean and variance given by the corresponding eigenvalue.

Figs. 3 and 4 illustrate the results of the numerical experiments. For Fig. 3a, the optimal model was fitted to exact data for the five-element array of Fig. 1, assuming spectral degrees of freedom $\nu = 30$, 180 and ∞ and $\hat{S} = \frac{1}{2}\pi$. In each case, the solution has been pushed as close to $\hat{S}$ (by the variational principle inherent in the model) as the constraint $\epsilon^{\mathrm{T}}\mathbf{V}^{-1}\epsilon = \rho_\gamma^2$ will allow; since $\mathbf{V}^{-1}$ is proportional to ν, $|\epsilon|$ must diminish as ν increases, and the solution looks progressively more like the test spectrum. The $\nu = \infty$ case indicates the limit of the ability of the optimal model to recover this test spectrum, given this array and no *a priori* knowledge. Although the fit of the optimal model in the limit of zero statistical error is excellent, it is seen that the limited spatial sampling still allows the existence of weak side lobes.

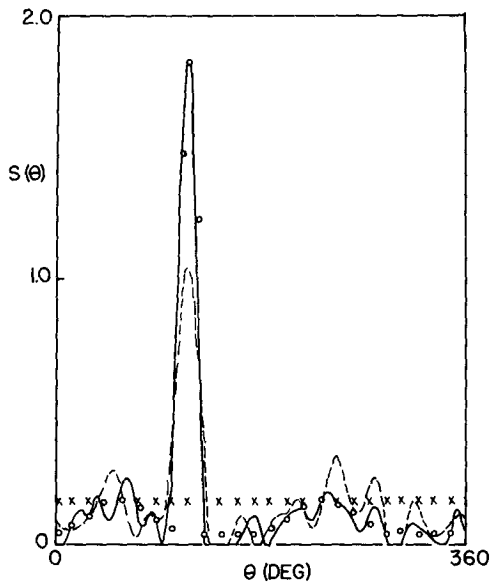

FIG. 5. Experiments with artificial noisy data. Input test spectrum (circles) is a sharp swell beam superposed on an undulating background. The favored model (crosses) is assumed isotropic. Dashed line, $\nu = 180$; solid line, $\nu = \infty$.

Fig. 3b shows the effect of a misleading choice for $\hat{S}$, in this case, a $\cos^{20}$ lobe identical in shape to S_W but centered at $\theta = 317°$, 180° away from the center of the S_W distribution. At 30 degrees of freedom, a second major lobe is allowed in the solution, in direct response to the erroneous $\hat{S}$ distribution. At $\nu = 180$, the constraint on $\epsilon^T \mathbf{V}^{-1} \epsilon$ tends to dominate, and the secondary lobe is largely attenuated.

Fig. 4 illustrates the effects of statistical noise in the data and a change in array geometry. For each of the four panels, three sets of statistically consistent artificial data were generated; in Figs. 4a and 4c for the five-element array of Fig. 1, and in Figs. 4b and 4d for the hypothetical six-element star array. The results reinforce the significance of noise in controlling model performance. At $\nu = 30$ (Figs. 4a and 4b) the optimal models differ rather grossly from the input test spectrum, and considerable variability exists between realization. The improved antenna beam pattern of the six-element star alters the results, but at this level of statistical uncertainty, the performance of the star is not obviously superior. At $\nu = 180$ the variability between solutions for the different realizations is much attenuated, and the agreement with the true model greatly improved. The performance of the six-element star is clearly superior to that of the five-element array, particularly with respect to side lobe suppression.

Finally, Fig. 5 shows the optimal model fit to the test spectrum S_S, for the six-element star array for noise-free data, $\nu = \infty$, and noisy data, $\nu = 180$, taking $\hat{S} = 1/2\pi$. Despite the presence of a peak considerably sharper than the classical antenna resolution, the optimal model agrees very well with the true distribution in the noise-free case. However, the addition of relatively weak noise results in a significant deterioration of the fit.

In conclusion, it appears that the side lobes occurring in the directional distributions of the real data cases shown in the examples of Figs. 2a and 2b are a consequence of the array geometry in conjunction with the noisiness of the spectral estimates. Much improved fits can be expected for longer time series, yielding a larger number of degrees of freedom.

6. Summary and conclusions

We have considered the problem of estimating a function (specifically, the directional spectrum of a gravity wave field) from measurements of integral properties of that function when those measurements are subject to statistical variability. Given the true spectrum, the statistical properties of the data errors are known, and a test of the hypothesis that any given model S is the true spectrum can be formulated. The appropriate measure of the fit of the model to the data is the quantity $\rho^2 = \epsilon^T \mathbf{V}^{-1} \epsilon$, where ϵ is the vector of implied statistical errors in the data and $\mathbf{V}^{-1}$ is the inverse of the error covariance matrix. This quantity is distributed as X_μ^2, where μ is the number of linearly independent measurements in the data set. It is then possible to establish a critical value of ρ^2 beyond which the valid model hypothesis must be rejected at any specified level of confidence.

For any data set, there exists in general an infinity of valid models; of these, we have defined as optimal that one which minimizes some (arbitrarily chosen) positive definite integral property of the model (and in addition satisfies the side condition that the distribution is not negative). One such property, $\int_0^{2\pi} d\theta (S - \hat{S})^2$, where $\hat{S}$ is some favored model, has been examined in detail, and the resulting procedure, applied to gravity wave-gage arrays, has been used both to analyze real data and to explore the subset of valid models under varying conditions in a series of numerical experiments. For weak noise levels, good results were obtained for a variety of directional spectra, including distributions considerably sharper than the classical antenna pattern of the array. The fit is relatively insensitive to the choice of $\hat{S}$. However, the quality of fit is strongly dependent on the statistical stability of the spectral estimates, indicating that good directional resolution from multicomponent arrays requires considerably longer time series than are customarily used for one-dimensional frequency spectra.

Although the subject has been treated largely in the context of surface gravity wave spectra, the ideas presented are applicable to any problem in-

volving the fitting of models to statistical data which estimate integral properties of the model.

Acknowledgments. The JONSWAP wave data were kindly made available through Karl Richter of the Deutsches Hydrographisches Institut and were spectral analyzed by Wolfgang Rosenthal, Institut für Geophysik, Universität Hamburg, and Hans-Jürgen Rubach, Deutsches Hydrographisches Institut. The work was carried out while the senior author was visiting the Max-Planck-Institut für Meteorologie.

REFERENCES

Backus, G. E., and J. F. Gilbert, 1967: Numerical applications of a formalism for geophysical inverse problems. *Geophys. J. Roy. Astron. Soc.* **13**, 247–276.

Barber, N. F., 1963: The directional resolving power of an array of wave detectors. *Ocean Wave Spectra*, Prentice-Hall, 357 pp.

Hasselmann, K., T. P. Barnett, E. Bouws, H. Carlson, D. E. Cartwright, K. Enke, J. A. Ewing, H. Gienapp, D. E. Hasselmann, P. Krusemann, A. Meerburg, P. Müller, D. J. Olbers, K. Richter, W. Sell and H. Walden, 1973: Measurement of wind-wave growth and swell decay during the Joint North Sea Wave Project (JONSWAP). *Deutsch. Hydrogr. Z.* (Suppl.), **A12**, 95 pp.

Jenkins, G. M., and D. G. Watts, 1968: *Spectral Analysis and its Applications*. Holden-Day, 525 pp.

Long, R. B., 1973: Scattering of surface waves by an irregular bottom. *J. Geophys. Res.* **78**, 33, 7861–7870.

Mitsuyasu, H., F. Tasai, T. Suhara, S. Mizuno, M. Ohkusu, T. Honda, and K. Rikiishi, 1975: Observations of the directional spectrum of ocean waves using a cloverleaf buoy. *J. Phys. Oceanogr.*, **5**, 750–760.

Olbers, D. J., P. Müller, and J. Willebrand, 1976: Inverse technique analysis of a large data set. *Phys. Earth Planet. Inter.*, **12**, 248–252.

Shemdin, O., K. Hasselmann, K. Herterick, and V. Hsiao, 1979: Nonlinear and linear bottom interaction effects in shallow water. *Proc. NATO Symp. Turbulent Fluxes through the Sea Surface, Wave Dynamics, and Prediction* (in preparation).